

Thermolytic Growth of ZnO Nanocrystals: Morphology Control and Optical Properties

Gerardo Muñoz-Hernández, Alejandro Escobedo-Morales, and Umapada Pal*

Instituto de Física, Benemérita Universidad Autónoma de Puebla, Apdo. Postal J-48, C.P. 72570, Puebla, Pue., Mexico

Received May 8, 2008; Revised Manuscript Received August 6, 2008

ABSTRACT: ZnO nanostructures with triangular and rod-like morphologies could be grown by thermolysis of zinc acetate in oleylamine solvent using oleic acid as surfactant. Concentration of the zinc precursor in the reaction mixture had a strong effect on the final morphology of the ZnO nanostructures. While a low precursor concentration results in triangular morphology, high precursor concentrations favor rod-like morphologies of the nanostructures. The room temperature photoluminescence (PL) spectra of both nanostructures are dominated by the green emission attributed to the oxygen vacancy (V_O) related donor–acceptor transition. Presence of several infrared (IR) inactive vibrational modes in the Fourier transform infrared (FT-IR) absorption spectra of the samples indicates a breakdown of translational symmetry in the nanostructures induced by native defects. Possible mechanisms of the morphology evolution and the origin of observed visible emissions in the nanostructures are discussed.

Introduction

Zinc oxide (ZnO) has attracted immense research interest worldwide during the present decade. Its wide band gap (3.37 eV)¹ and high exciton binding energy (60 meV)² make it a potential material for the applications in optoelectronic devices. In this regard, developing a low cost process to control the morphology and optical properties is the main challenge to build ZnO nanostructure-based technologies. It is well-known that by reducing the size of materials their properties can be modified drastically.^{3–7} Considerable efforts have been devoted to control the morphology and size of ZnO nanostructures.^{8–11} Nevertheless, the synthesis methods to obtain controlled nanostructures often involve tedious processes.¹² Generally, morphology control in metal oxide nanostructures requires chemical methods using highly alkaline solutions,^{13,14} or physical methods performing at high temperatures.^{15–17} However, use of a low temperature soft chemical method for fabricating metal oxide nanostructures with controlled and versatile morphology is essential for their low cost production.

On the other hand, fabrication of morphology-controlled metal oxide nanostructures is not a unique requirement to use them as a basic material for optoelectronic devices. It also requires a vast understanding of optical phenomena observed in such materials.

The origin of electronic transitions responsible for observed visible luminescence in ZnO has been a topic of extensive research recently. Nevertheless, the origin of such emissions remains controversial.

In the present article, we report the synthesis of well crystallized ZnO nanostructures with controlled morphology simply through the thermolysis of zinc acetate at relatively low temperature. Through this technique, nanotriangles or nanorods could be synthesized by a precise variation of the concentration of zinc precursor salt. Morphology and growth structure of the nanostructures were studied by transmission electron microscopy (TEM). Optical properties of the obtained ZnO nanostructures were studied by room temperature photoluminescence and infrared spectroscopy techniques. Possible origin of observed

Table 1. Amounts of Zinc Precursor Salt, Oleic Acid, and Oleylamine Used in Different Synthesis Processes and Corresponding Resulting Morphologies

sample	zinc acetate (mmol)	oleic acid (mmol)	oleylamine (mmol)	zinc acetate (M) oleic acid (M)	morphology
A	3.75	30	76	0.125	nanotriangles
B	7.5	30	76	0.25	nanotriangles
C	15	30	76	0.50	nanotriangles and nanorods
D	30	30	76	1.0	nanorods
E	60	30	76	2.0	nanorods

luminescence emissions and the mechanism of morphology control are discussed.

Experimental Section

For the synthesis of ZnO nanostructures, zinc acetate dihydrate [$Zn(CH_3COO)_2 \cdot 2H_2O$, J.T. Baker, 99.6%], oleic acid ($C_{18}H_{34}O_2$, technical grade 90%, Aldrich), and oleylamine ($C_{18}H_{37}N$, technical grade 70%, Aldrich) were purchased and used without further purification. In a typical synthesis process, 76 mmol of oleylamine (solvent) and 30 mmol of oleic acid (surfactant) were mixed in a round-bottom flask under vigorous stirring. In order to eliminate the humidity in the reaction flask, a nitrogen gas flux was applied throughout the reaction process. To control the morphology of the ZnO nanostructures, specific amounts of zinc acetate (3.75, 7.5, 15, 30, and 60 mmol) were added to the surfactant and solvent-containing flask. In this way, the molar ratio of zinc precursor and oleic acid was varied from 0.125 to 2.0. Once the zinc salt was dissolved in the solution, it was gradually heated up to 220 °C. After several minutes at this temperature, the reaction mixture turned white. After about 15 min of heating at this temperature, the product was cooled down to room temperature. Then the white material was centrifuged and washed several times with hexane. ZnO nanostructures were characterized by X-ray diffraction (XRD) (Bruker axS D8 Discover, $Cu K\alpha = 1.5406 \text{ \AA}$), low and high resolution transmission electron microscopy (TEM and HRTEM) (JEOL JEM-2010F), room temperature photoluminescence (PL) (325 nm line of a Melles Griot He–Cd laser; 0.5 m ScienceTech 9040 monochromator), and Fourier transform infrared spectroscopy (FT-IR) (Nicolet 750 with a DTGS detector). The acquired PL spectra of the samples were corrected using the spectral responses of the monochromator and the detector (Photomultiplier, ScienceTech PMH-04).

Results and Discussion

Table 1 summarizes the relative molar quantities of zinc acetate dihydrate, oleylamine, and oleic acid used to obtain the

* Corresponding author: Tel.: +52 222 295500 ext. 2047; fax: +52 222 295611, e-mail: upal@sirio.ifuap.buap.mx.

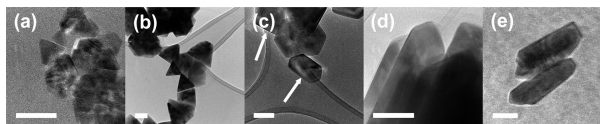


Figure 1. Typical TEM images of the samples grown with different molar ratios of zinc acetate and oleic acid: (a) 0.125, (b) 0.25, (c) 0.50, (d) 1.0, and (e) 2.0. All the scale bars correspond to 100 nm. Arrows in Figure 1c point to triangular and rod-like nanostructures.

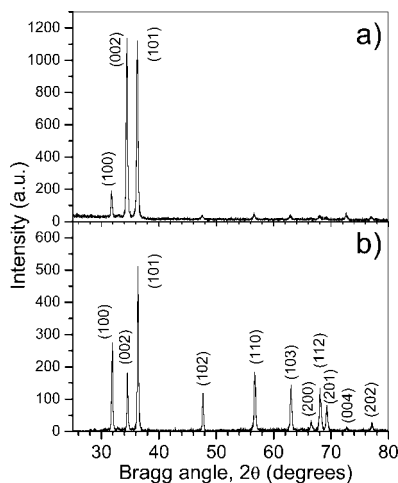


Figure 2. XRD patterns of wurtzite ZnO: (a) nanotriangles, and (b) nanorods.

ZnO nanostructures. It was observed that the resulting morphology of ZnO nanostructures has a strong dependence on the molar concentration of zinc precursor salt and surfactant (oleic acid). While low precursor to surfactant ratios (0.125 and 0.25) produce ZnO nanotriangles, an increase in concentration of zinc acetate results in a few ZnO nanorod structures mixed with nanotriangles. Upon increasing the concentration of zinc salt further (1.0 and 2.0 molar ratios), only nanorods are obtained. Figure 1 shows typical TEM images of the nanostructures grown with different concentrations of zinc acetate. It is clear that at low precursor concentration, triangular morphology is favored. Upon increasing the precursor concentration, both triangular and rod-like morphologies appeared. For even higher concentrations of the precursor, only rod-like morphology was formed. Possible growth mechanisms of such nanostructures and their morphological evolution are discussed later.

For detailed structural and optical studies, sample B (zinc acetate and oleic acid molar ratio = 0.25) and sample D (zinc acetate and oleic acid molar ratio = 1.0) were taken as representative materials of nanotriangles and nanorods, respectively. Figure 2 shows the XRD patterns of nanotriangles and nanorods. Observed diffraction peaks revealed that both nanotriangles and nanorods are wurtzite ZnO ($P6_3mc$, $a = 3.249 \text{ \AA}$, $c = 5.206 \text{ \AA}$, JCPDS No. 36-1451). It is interesting to note that the XRD pattern of ZnO nanotriangles has a (002) plane reflection more intense than a (101) reflection, which suggests a preferential orientation of the nanostructures along the [001] direction. The XRD pattern of nanorods is similar to that expected in a polycrystalline sample with random orientation.

Figure 3 shows low and high magnification TEM images of nanotriangles and nanorods. In Figure 3a, equilateral triangles of about 200 nm base size can be observed. Also several nanotriangles (marked) join to form a structure similar to a half-hexagon. The growth mechanism of such nanostructures has been reported previously by Zhang et al.¹⁸ A typical HRTEM

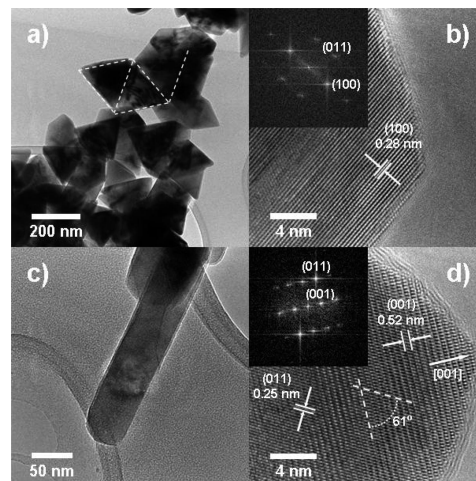


Figure 3. (a) Low magnification TEM micrograph of nanotriangles. (b) HRTEM image of the corner of a selected nanotriangle, with corresponding FFT pattern as inset. (c) Low magnification TEM micrograph of nanorods. (d) typical HRTEM image of a nanorod with corresponding FFT pattern of a selected area.

image of a corner of a nanotriangle is shown in Figure 3b. The measured interplanar spacing of 0.28 nm matches with the interplanar spacing of (100) planes of wurtzite ZnO. The fast Fourier transform (FFT) of the image (inset Figure 3b) confirms that the crystal is oriented through the [001] crystallographic direction; i.e. the sides of the nanotriangle are composed of a {100} family of planes and the triangular face corresponds to the (001) plane. Figure 3c shows the TEM micrograph of a nanorod with 70 nm in diameter and about 100 nm in length. From the typical HRTEM image of a tip of a nanorod presented in Figure 3d, two interplanar spacings can be determined. The interplanar spacing of 0.25 and 0.52 nm corresponds to the (101) and (001) planes, respectively, with about a 61° angle between them, in agreement with wurtzite ZnO structure. The FFT pattern of the HRTEM image (inset Figure 3d) indicates that the nanorod structures grow along the [001] direction, by subsequent stacking of (001) planes and a restrictive growth of {100} family planes.

Formation of resulting morphologies of ZnO nanostructures can be understood through the interaction of zinc oxide seeds with the surfactant. The polar nature of oleic acid molecule favors its adsorption on the (001) polar plane of zinc oxide. It is expected that at lower molar ratios of zinc precursor and oleic acid (0.125 and 0.25) a higher amount of surfactant molecules are attached on the (001) plane, inhibiting its growth by decreasing the surface free energy. Restrictive growth of the (001) plane favors the ZnO seeds to grow along the (100), (0-10), and (-110) lateral planes, resulting in the observed triangular morphology. On the other hand, if the concentration of zinc precursor is further increased (1.0 and 2.0), there is not enough oleic acid molecules adsorbed on the (001) plane to restrict its growth process. Therefore, the ZnO seed follows its preferential growth along the c -axis, producing observed rod-like ZnO morphology. Figure 4 summarizes the obtained morphology of ZnO nanostructures with respect to zinc acetate concentration, along with some models of preferential growth planes.

In order to study the effect of morphology on the optical properties of ZnO nanostructures, they were characterized by FT-IR and PL spectroscopy at room temperature. Figure 5 shows the FT-IR spectra of nanotriangles (Figure 5a) and nanorods (Figure 5b). Several absorption bands besides those attributed

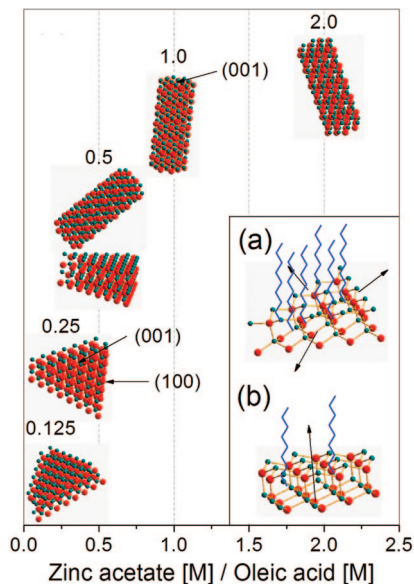


Figure 4. Variation of morphology of ZnO nanostructures with the variation of zinc acetate and surfactant molar ratio. Insets show schematic models of (a) nanotriangle and (b) nanorod growth processes. Oleic acid molecules are represented by zigzag chains. Surfactant molecules attached at {100} planes are not shown for simplicity. Preferential growth directions are indicated by arrows.

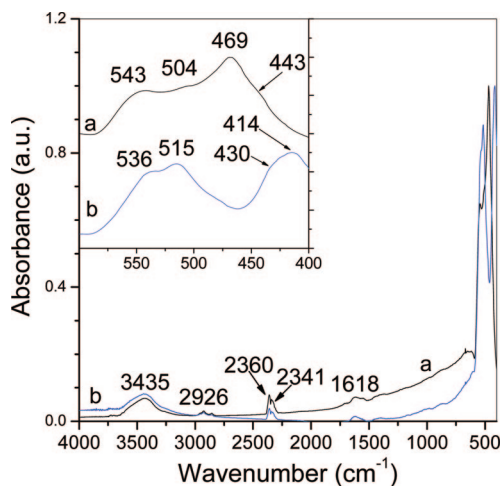


Figure 5. Infrared spectra of ZnO (a) nanotriangles and (b) nanorods. Inset shows the IR spectra in the frequency range where the vibrational modes of wurtzite ZnO are observed.

to ZnO vibrational modes appeared in the FT-IR spectra of both samples at about 3435, 2926, 2360, 2341, and 1618 cm^{-1} . The bands at 3435 and 1618 cm^{-1} are attributed to the stretching and bending modes of the hydroxyl group (OH) of water molecules adsorbed on the surface of nanostructures, respectively. Absorption of carbon dioxide molecules present in the atmosphere corresponds to bands located at 2360 and 2341 cm^{-1} . The band at 2926 cm^{-1} is attributed to the asymmetric stretching mode of the CH_2 group of oleic acid,¹⁹ which was not completely removed by washing and centrifugation with hexane. The inset of Figure 5 shows the FT-IR spectra of the samples in the frequency range where vibrational modes related to ZnO are observed. For nanorods (spectrum b of the inset of Figure 5), four bands located at about 536, 515, 430, and 414 cm^{-1} are observed. The band at 414 cm^{-1} can be assigned to the infrared active E_1 -TO mode of ZnO;²⁰ nevertheless, the other

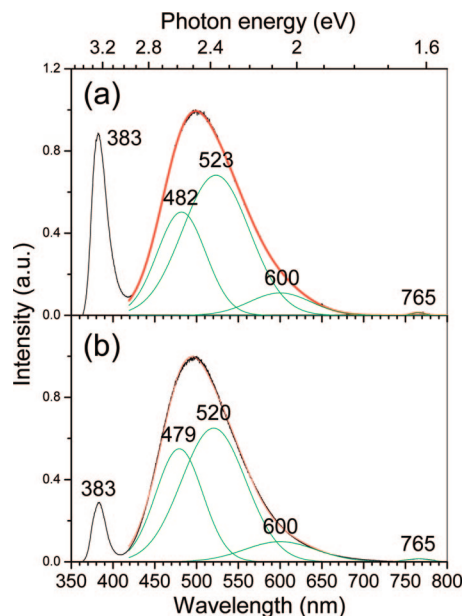


Figure 6. Room temperature PL spectra of the (a) ZnO nanotriangles, and (b) ZnO nanorods. Broad visible emission band is deconvoluted in several Gaussian functions for further analysis.

bands do not match with any IR-active vibrational mode for bulk ZnO. Several authors have reported similar anomalous vibrational modes in ZnO^{21–23} attributed to local vibrational modes of impurities or defects. Manjón et al.²⁴ have demonstrated that most of these modes correspond to silent modes allowed by the breakdown of the translational symmetry induced by native defects. On the other hand, if the translational symmetry is broken at certain point defects, it is feasible that frequencies close to the symmetric modes can be observed not only by Raman spectroscopy but also in their IR spectra. Therefore, activation of silent modes by native defects can be the origin of the band located at 515 cm^{-1} , while the band at about 430 cm^{-1} can be assigned to the Raman-active E_2 -high mode.²⁵ It is interesting to note that the bands at about 536 and 430 cm^{-1} differ by about 106 cm^{-1} , which matches with the frequency of the Raman-active E_2 -low mode ($\sim 102 \text{ cm}^{-1}$).²⁶ Therefore, the band at about 536 cm^{-1} is probably a second-order vibrational mode involving E_2 -high and E_2 -low modes.

The infrared spectrum of the nanotriangles (inset Figure 5a) reveals four bands centered at about 543, 504, 469, and 443 cm^{-1} . It is interesting to note that the E_1 -TO mode ($\sim 414 \text{ cm}^{-1}$) is absent in this case due to the preferred orientation of nanostructures along c -axis.²⁷ Instead of E_1 -TO mode, a shoulder at about 443 cm^{-1} appeared which can be attributed to E_2 -high mode. Gupta et al.²⁷ have reported experimental observation of surface phonon modes at frequencies near to 470 cm^{-1} in ZnO nanostructures with high surface-to-volume ratio. The band observed at 469 cm^{-1} corresponds to the lower surface phonon mode enhanced due to the high surface-to-volume ratio of nanotriangles. Similar to the nanorods, the bands at 504 and 543 cm^{-1} in the triangular structures are tentatively attributed to the activation of a silent mode and the second order of E_2 modes, respectively.

Room temperature PL spectra of the ZnO nanostructures are shown in Figure 6. The PL spectra of both samples (nanotriangles and nanorods) are composed of a UV band located at about 383 nm (3.24 eV), attributed to recombination of free excitons, a broad visible emission band attributed to native defects of ZnO, and a near IR band located at about 765 nm

(1.62 eV). It can be seen that the intensity of the excitonic emission band is higher in nanotriangles, which suggests their better crystallinity over the nanorods. To analyze the broad visible emission band in detail, it was deconvoluted into several Gaussian functions. On deconvolution, a blue band (480 nm, 2.58 eV), a green band (520 nm, 2.38 eV), and a yellow band (600 nm, 2.07 eV) were revealed. The positions and relative intensities of these component bands are similar for both the samples. The broad visible defect emission bands in both samples are dominated by the green band, which has been related to the oxygen vacancies (V_O) by several authors.^{28–30} We propose that the green emission band is due to the electronic transition between a donor level (V_O) and an electronic level generated by zinc vacancies (V_{Zn}). As the oxygen vacancies (V_O) and interstitial zinc (Zn_i) are reported to be the predominant intrinsic defects in ZnO,^{31–33} it is feasible that the predominant visible emission involves such native defects. On the other hand, there are relatively few reports concerning the origin of blue emission bands in ZnO. Cheng et al.³⁴ have attributed the blue emission to V_O native defects.

The yellow emission in ZnO has already been attributed to oxygen excess.³⁰ We believe that the yellow band at 550 nm involves recombination of an electron located in the conduction band and a hole at O_i level. Finally, the weak near IR emission band located at about 765 nm is possibly the second order of the free exciton (FX) emission, as on decreasing the intensity of the FX emission in the rod-like sample, the intensity of this peak reduces.

Conclusions

By adjusting the molar concentration of zinc precursor, ZnO nanostructures of different morphologies could be grown in a relatively low temperature thermolysis process using oleic acid as surfactant. The evolution of morphologies in the process could be understood by considering the interactions of polar surfactant with the crystal planes of ZnO at the initial stage of their growth. While the highly crystalline triangular ZnO nanostructures grow perpendicular to the [001] direction, the rod-like nanostructures grow along the [001] direction by stacking (001) planes one over other. Absence of the E_1 -TO mode in the ZnO nanostructures of triangular morphology and the presence of IR-silent local vibrational modes for both the morphologies are due to preferred c -axis orientation and the breakdown of translational symmetry induced by native defects, respectively.

While the appearance of excitonic emission in the PL spectra for both morphologies indicates their good crystalline quality, the presence of broad visible emission dominated by the green emission band indicates the presence of several point defects like oxygen vacancy (V_O), zinc vacancy (V_{Zn}), zinc interstitial (Zn_i), and oxygen interstitial (O_i) in the nanostructures.

Acknowledgment. We are thankful to Luis Rendon, LCM-UNAM, for his help in acquiring TEM and HRTEM images of the nanostructures. This work was partially supported by CONACyT, Mexico (grant no. 46269) and VIEP-BUAP (grant no. VIEP/EXC/93/2008-1).

References

- (1) Chen, Y. F.; Bagnall, D. M.; Koh, V.; Park, K.; Hiraga, K.; Zhu, Z.; Yao, T. *J. Appl. Phys.* **1998**, *84*, 3912–3918.
- (2) Liang, W. Y.; Yoffe, A. D. *Phys. Rev. Lett.* **1968**, *20*, 59–62.
- (3) Maulenkamp, E. A. *J. Phys. Chem. B* **1998**, *102*, 5566–5572.
- (4) Chen, W.; Malm, J. O.; Zwiller, V.; Wallenberg, R.; Bovin, J. O. *J. Appl. Phys.* **2001**, *89*, 2671–2675.
- (5) Rajalakshmi, M.; Arora, A. K.; Bendre, B. S.; Mahamuni, S. *J. Appl. Phys.* **2000**, *87*, 2445–2448.
- (6) Matsumoto, T.; Kato, H.; Miyamoto, K.; Sano, M.; Zhukov, E. A.; Yao, T. *Appl. Phys. Lett.* **2002**, *81*, 1231–1233.
- (7) Wang, J.; An, X.; Li, Q.; Egerton, R. F. *Appl. Phys. Lett.* **2005**, *86*, 201911.
- (8) Zhou, H.; Wissinger, M.; Fallert, J.; Hauschild, R.; Stelzl, F.; Klingshirn, C.; Kalt, H. *Appl. Phys. Lett.* **2007**, *91*, 181112.
- (9) Kang, B. S.; Pearton, S. J.; Ren, F. *Appl. Phys. Lett.* **2007**, *90*, 083104.
- (10) Hartlieb, K. J.; Raston, C. L.; Saunders, M. *Chem. Mater.* **2007**, *19*, 5453–5459.
- (11) Chung, T. F.; Luo, L. B.; He, Z. B.; Leung, Y. H.; Shafiq, I.; Yao, Z. Q.; Lee, S. T. *Appl. Phys. Lett.* **2007**, *91*, 233112.
- (12) Murray, C. B.; Norris, D. J.; Bawendi, M. G. *J. Am. Chem. Soc.* **1993**, *115*, 8706–8715.
- (13) Du, G. H.; Chen, Q.; Che, R. C.; Yuan, Z. Y.; Peng, L. M. *Appl. Phys. Lett.* **2001**, *79*, 3702–3704.
- (14) Yan, T.; Liu, X. L.; Wang, N. R.; Chen, J. F. *J. Cryst. Growth* **2005**, *281*, 669–677.
- (15) Wang, Y. G.; Yuen, C.; Lau, S. P.; Yu, S. F.; Tay, B. K. *Chem. Phys. Lett.* **2003**, *377*, 329–332.
- (16) Li, S. Y.; Lin, P.; Lee, C. Y.; Tseng, T. Y. *J. Appl. Phys.* **2004**, *95*, 3711–3716.
- (17) Han, X.; Wang, G.; Wang, Q.; Cao, L.; Liu, R.; Zou, B.; Hou, J. G. *Appl. Phys. Lett.* **2005**, *86*, 223106.
- (18) Zhang, J.; Liu, H.; Wang, Z.; Ming, N. *Appl. Phys. Lett.* **2007**, *90*, 113117.
- (19) Wu, N.; Fu, L.; Su, M.; Aslam, M.; Wong, K. C.; Vinayak, P. D. *Nano Lett.* **2004**, *4*, 383–386.
- (20) Venger, E. F.; Melnichuk, A. V.; Melnichuk, L. L.; Pasechnik, Y. A. *Phys. Status Solidi B* **1995**, *188*, 823–831.
- (21) Tzolov, M.; Tzenov, N.; Malinowska, D. D.; Kalitzova, M.; Pizzuto, C.; Vitali, G.; Zollo, G.; Ivanov, I. *Thin Solid Films* **2000**, *379*, 28–36.
- (22) Kacsner, A.; Haboeck, U.; Strassburg, M.; Strassburg, M.; Kaczmarczyk, G.; Hoffmann, A.; Thomsen, C.; Zeuner, A.; Alves, H. R.; Hofmann, D. M.; Meyer, B. K. *Appl. Phys. Lett.* **2002**, *80*, 1909–1911.
- (23) Bundesmann, C.; Ashkenov, N.; Schubert, M.; Spemann, D.; Butz, T.; Kaidashev, E. M.; Lorenz, M.; Grundmann, M. *Appl. Phys. Lett.* **2003**, *83*, 1974–1976.
- (24) Manjón, F. J.; Marí, B.; Serrano, J.; Romero, A. H. *J. Appl. Phys.* **2005**, *97*, 053516.
- (25) Arguello, C. A.; Rousseau, D. L.; Porto, S. P. S. *Phys. Rev.* **1969**, *181*, 1351–1363.
- (26) Özgür, Ü.; Alivov, Y. I.; Liu, C.; Teke, A.; Reshchikov, M. A.; Doan, S.; Avrutin, V.; Cho, S. J.; Morkoç, H. *J. Appl. Phys.* **2005**, *98*, 041301.
- (27) Gupta, V.; Bhattacharya, P.; Yuzuk, Y. I.; Sreenivas, K.; Katiyar, R. S. *J. Cryst. Growth* **2006**, *287*, 39–43.
- (28) Vanheusden, K.; Warren, W. L.; Seager, C. H.; Tallant, D. R.; Voigt, J. A.; Gnade, B. E. *J. Appl. Phys.* **1996**, *79*, 7983–7990.
- (29) Hu, Y.; Chen, H. J. *J. Appl. Phys.* **2007**, *101*, 124902.
- (30) Studenikin, S. A.; Golego, N.; Cocivera, M. *J. Appl. Phys.* **1998**, *84*, 2287–2294.
- (31) Kohan, A. F.; Ceder, G.; Morgan, D.; Van de Walle, C. G. *Phys. Rev. B* **2000**, *61*, 15019–15027.
- (32) Zhang, S. B.; Wei, S. H.; Zunger, A. *Phys. Rev. B* **2001**, *63*, 075205.
- (33) Sokol, A. A.; French, S. A.; Bromley, S. T.; Catlow, C. R. A.; van Dame, H. J. J.; Sherwoode, P. *Faraday Discuss.* **2007**, *134*, 267–282.
- (34) Cheng, W.; Wu, P.; Zou, X.; Xiao, T. *J. Appl. Phys.* **2006**, *100*, 054311.

CG8004807